Hindawi
International Journal of Antennas and Propagation
Volume 2022, Article ID 1017206, 9 pages
https://doi.org/10.1155/2022/1017206

Research Article

Two-Step Frequency Estimation of GNSS Signal in High-Dynamic Environment

Chao Wu,[1,2] **Yafeng Li**,[3] **Liyan Luo**,[4] **Jian Xie**,[2] **and Ling Wang**[2]

[1]*School of Communication Engineering, Hangzhou Dianzi University, Hangzhou 310018, China*
[2]*School of Electronic Information, Northwestern Polytechnical University, Xi'an 710072, China*
[3]*School of Automation, Beijing Information Science and Technology University, Beijing100192, China*
[4]*Provincial Ministry of Education Key Laboratory of Cognitive Radio and Signal Processing, Guilin University of Electronic Technology, Guangxi 541004, China*

Correspondence should be addressed to Chao Wu; wuchaoid@126.com

Received 8 April 2022; Revised 20 June 2022; Accepted 21 June 2022; Published 7 July 2022

Academic Editor: Atsushi Mase

To improve frequency accuracy which is affected by two parameters in high-dynamic acquisition, we propose a two-step frequency estimation method based on the mean frequency (MF) model for high-dynamic parameters estimation. The first step is based on the discrete chirp-Fourier transform (DCFT) for coarse MF estimation, where the MF accuracy and frequency search step are derived. In the second step, the maximum likelihood estimation process (MLEP) is adopted for fine MF estimation. Compared with state-of-art methods, it is verified that the two-step method can improve the detection probability in coarse MF estimation and improve the MF accuracy with low computational burdens under conditions with a moderate signal-to-noise ratio (SNR).

1. Introduction

In global navigation satellite system (GNSS) receiver techniques, the acquisition is the most important process for estimating code phase and carrier frequency [1]. For fast acquisition with lower computational complexity, the method [2–4] based on fast Fourier transform (FFT) was proposed. Since the pull-in range of the tracking loop is only a few hertz, the number of FFT points should be increased [5]. Generally, the coarse-to-fine acquisition methods are used to reduce the computation costs [6]. The code phase and coarse carrier frequency parameters can be obtained from the coarse acquisition, and the carrier frequency can be refined in a specific fine acquisition process with the code stripped off.

For low-dynamic acquisition, the carrier Doppler can be estimated in the fine acquisition process. Tang et al. [7] proposed an accurate estimation method for residual Doppler. However, this method has a restriction on the initial Doppler search step, and more computation is required to obtain an accurate Doppler. To reduce computational load, a method [8] was proposed based on the coarse Doppler and sampling frequency in moderate SNR. However, to improve the Doppler accuracy in low SNR, a long-time correlation process is typically needed, which costs a lot of computations. To reduce the computations with long integration, Mohamed and Aboelmagd [5] proposed the Schmidt method which utilizes orthogonal searching. To further reduce the computations, article [9] proposed the zero-forcing and a double FFT-based method to improve Doppler frequency accuracy without increasing the computational load. However, because of the trade-off between the Doppler frequency resolution and the computational complexity, the maximum error of carrier frequency estimation depends on the number of FFT points. To improve the Doppler frequency accuracy, Nguyen et al. [10] proposed a residual frequency estimation method with differential processing. Due to the differential processing, it performs not well in the low SNR.

Above all, the articles listed only focus on Doppler frequency accuracy. However, both initial frequency and chirping rate [11] affect the correlation peak in high-

dynamic applications. Moreover, with a long integration time, the influence of these two parameters cannot be ignored. Among methods for initial frequency and chirping rate estimation, the authors in [12, 13] proposed frequency estimation methods based on Fractional Fourier transform (FRFT) for high-dynamic applications. In addition, we proposed a frequency estimation method based on discrete chirp-Fourier transform (DCFT) [14]. However, in some high-dynamic applications, more accurate frequency is usually desired.

To further improve frequency accuracy for high-dynamic applications, a two-step frequency parameter estimation method is proposed in this paper. An MF model has been derived to improve the frequency accuracy. In the first step for coarse MF estimation, the chirping rate and initial frequency for MF estimation have been estimated based on the DCFT. A maximum likelihood estimation process (MLEP) has been proposed for the fine MF estimation in the 2nd step. With the two-step processing, the computational burdens can be reduced when the peak value is smaller than the configured threshold, and high-frequency accuracy can be obtained when the signal is present. Simulation results show that for coarse MF estimation, the proposed method has a higher detection probability compared with conventional methods, and for fine MF estimation, the two-step method has a higher frequency accuracy and lower computational burdens than the compared methods.

2. Signal Model

After correlating with a one-period local code and a coarse Doppler bin [11], the postcorrelation signal can be obtained and depicted as follows:

$$S(n) = Ab(n)\exp\left[j2\pi\left(f_0 nT_s + \mu n^2 T_s^2\right)\right] + W(n), \quad (1)$$

where f_0 represents residual Doppler frequency or initial frequency, μ represents the chirping rate or Doppler rate, T_s represents the sampling frequency, $b(n)$ represents bit sign, A represents signal amplitude, and $W(n)$ denotes a zero-mean additive white Gaussian noise (AWGN) process. When the received signal is not aligned with local code or a wrong Doppler bin is detected, signal amplitude $A \approx 0$, which is called the signal-absent situation in the following analysis. Or, $A \neq 0$ is assumed as a constant 11. For GPS L1 CA signal with 1-ms code period, it is typical that $f_0 = (-250, 250)$ Hz, and $\mu = (-500, 500)$ Hz/s. It is assumed that $b(n)$ can be obtained by some auxiliary means 13, and $b(n)$ equals 1 in the following analysis.

3. Proposed Method

In this section, the process based on DCFT has been proposed for coarse MF estimation. Then, MLEP has been adopted for fine MF estimation. Finally, the two-step method which combines the two processes has been proposed. In this two-step method, signal detection and MF accuracy improvement are realized through the first and second steps respectively.

3.1. Coarse Search of MF Based on DCFT. T transform of the postcorrelation signal can be written as follows:

$$S_T(k_T, \alpha_T) = A_T \sum_{n=0}^{N-1} b(n)\exp\left\{j2\pi\left[\Delta_T n T_s + \delta_T n^2 T_s^2\right]\right\} + w, \quad (2)$$

where $k_T = 0, \pm 1, \pm 2, \ldots$ represents a searching range, and α_T represents transform factor. $w = w_i + jw_r$. w_i and w_r both obey normal distribution $N(0, \sigma_w^2)$. When $T=f$, it represents FRFT [15]. $A_f = A\exp[-j\pi\mathrm{sgn}(\sin\alpha_f)/4 + j\alpha_T/2]/\ |\sin\alpha_f|^{0.5} \exp[j1/2\cot\alpha_f (kF)^2]$. $F = 2\pi/NT_s\csc\alpha_f$. $\Delta_f = (f_0 - k_f/NT_s)$. $\delta_f = (\mu + 1/4\pi\cot\alpha_f)$. When $T=d$, it represents DCFT. $A_d = A$. $\Delta_d = (f_0 - k_d/NT_s)$. $\delta_d = (\mu - \alpha_d/N^2T_s^2)$, where α_d represents the chirping rate factor. Based on (2), the correlation peak of FRFT is an unilinear function with α_f, which may degrade the detection peak. Therefor DCFT is chosen in the following discussion.

When the bit signs can be obtained by assisted means, the formula above can be simplified into

$$\begin{aligned} S_d(k_d, \alpha_d) &\approx A_d \sum_{n=0}^{N-1} \exp\left[j\overline{\omega} n T_s\right] + w \\ &= A_d N \mathrm{sinc}\left(\frac{\overline{\omega} N T_s}{2}\right)\exp\left(j\overline{\omega}\frac{N-1}{2}T_s\right) + w, \end{aligned} \quad (3)$$

where N represents the integration time and $\overline{\omega} = 2\pi\Delta_T + 2\pi\delta_T(N-1)/2T_s$ represents the MF from $0T_s$ to $(N-1)T_s$. It is assumed that $A_0 = A_d N$. Based on the derivations above and Taylor expansion, the peak $|A_d\sum_{n=0}^{N-1}\exp[j\overline{\omega}nT_s]|$ can be approximated as

$$\begin{aligned} \left|A_d \sum_{n=0}^{N-1} \exp\left[j\overline{\omega} n T_s\right]\right| &= A_0\left|\mathrm{sinc}\left(\overline{\omega} N \frac{T_s}{2}\right)\right| \\ &\approx A_0\left[1 - \frac{1}{6}\left(\overline{\omega} N \frac{T_s}{2}\right)^2\right], \end{aligned} \quad (4)$$

where $|A_d\sum_{n=0}^{N-1}\exp[j\overline{\omega}nT_s]|$ represents the amplitude of the signal $A_d\sum_{n=0}^{N-1}\exp[j\overline{\omega}nT_s]$. It is assumed that the unit (k_{d0}, α_{d0}) is corresponding to the peak, and $|A_d\sum_{n=0}^{N-1}\exp[j\overline{\omega}nT_s]| \geq \gamma A_0$, where γ is set based on the criterion that one search bin contains mostly useful energy [16]. Then, we can obtain

$$\overline{\omega} \leq 2\sqrt{6(1-\gamma)}/(NT_s). \quad (5)$$

Based on the equations above, the search step of MF in the first step is set to $2\sqrt{6(1-\gamma)}/(NT_s)$. Due to the influence between the initial frequency and chirping rate, the search step of the initial frequency needs to be configured first. Based on the influence of residual Doppler frequency on the correlation peak value of the postcorrelation signal in low-dynamic applications [4], the search step of initial frequency is set to $1/(2NT_s)$. Moreover, based on the relationship between the initial frequency search step and the MF search step in the first step, the search step of the chirping rate can be obtained.

Above all, in the coarse search, the coarse estimations of both initial frequency and chirping rate can be obtained. Based on the coarse estimation, the coarse MF estimation can be obtained.

3.2. MLEP for Fine MF Estimation. In the MLEP, firstly, the signal amplitude is estimated based on ML; then, due to the fine MF range, the restricted search criteria for the fine MF estimation are adopted. Finally, combining the criteria and ML function, the fine MF is estimated based on the estimated signal amplitude.

Based on (3), the observed peak can be written as follows:

$$S_d(A_0, \overline{\omega}_0) = A_0 sinc\left(\frac{\overline{\omega}_0 NT_s}{2}\right)\exp\left(j\overline{\omega}_0 \frac{N-1}{2}T_s\right) + w, \quad (6)$$

where $\overline{\omega}_0$ represents residual MF, which ranges from $-\sqrt{6(1-\gamma)}/(NT_s)$ to $\sqrt{6(1-\gamma)}/(NT_s)$ based on Section 3.1 analysis. The joint probability density function of (w_i, w_r) of (w_i, w_r) can be written as

$$f(w_i, w_r) = \frac{1}{2\pi\sigma_w^2}\exp\left[-\frac{(w_i)^2 + (w_r)^2}{2\sigma_w^2}\right]. \quad (7)$$

Then, based on ML estimation, the optimized objective function can be obtained as

$$\min J(A_0, \overline{\omega}_0) = \min\left(-\ln\left(f(w_i, w_r)\right)\right) \approx \min\left(\frac{(w_i)^2 + (w_r)^2}{2\sigma_w^2}\right), \quad (8)$$

where $min\, J(A_0, \overline{\omega}_0)$ represents the minimum of the objective function $J(A_0, \overline{\omega}_0)$. It is assumed that $\partial J(A_0, \overline{\omega}_0)/\partial A_0 = 0$. Then, we can obtain

$$A_{0c} = \frac{\mathrm{Re}(S_d)\cos(\overline{\omega}_0 N - 1/2T_s) - \mathrm{Im}(S_d)\sin(\overline{\omega}_0 N - 1/2T_s)}{\mathrm{sinc}(\overline{\omega}_0 NT_s/2)\cos(\overline{\omega}_0(N-1)T_s)}, \quad (9)$$

where A_{0c} represents the optimized value of A_0 based on ML. Then, substituting (9) into (6), we can obtain

$$S_d(A_{0c}, \overline{\omega}_0) = \frac{\mathrm{Re}(S_d)\cos(\overline{\omega}_0 N - 1/2T_s) - \mathrm{Im}(S_d)\sin(\overline{\omega}_0 N - 1/2T_s)}{\cos(\overline{\omega}_0(N-1)T_s)} \cdot \exp\left(j\overline{\omega}_0 \frac{N-1}{2}T_s\right) + w, \quad (10)$$

where $S_d(A_{0c}, \overline{\omega}_0)$ represents the correlation peak in presence of noise. However, when $\cos(\overline{\omega}_0(N-1)T_s) = 0$, $\overline{\omega}_0 = \pi(2k+1)/(2(N-1)T_s)$ represents singular points of (10), $k = 0, \pm 1, \pm 2, \ldots$ represents segmentation variable, L_k represents the length of k. Consequently, the segmentation optimization is taken based on the singular points. When $\pi(2k+1)/(2(N-1)T_s) < \overline{\omega}_0 < \pi(2k+3)/(2(N-1)T_s)$, the segmentation optimization is based on the objective function as follows:

$$J(A_{0c}, \overline{\omega}_0 + \Delta\omega) = \frac{\left(w_i(\overline{\omega}_0 + \Delta\omega)\right)^2 + \left(w_r(\overline{\omega}_0 + \Delta\omega)\right)^2}{2\sigma_w^2} = \frac{\left(w_i(\overline{\omega}_0) + J_i\Delta\omega\right)^2 + \left(w_r(\overline{\omega}_0) + J_r\Delta\omega\right)^2}{2\sigma_w^2}, \quad (11)$$

where J represents the objective function. It is assumed that $\partial J(A_{0c}, \overline{\omega}_0 + \Delta\omega)/\partial\Delta\omega = 0$, $\Delta\omega$ can be obtained as follows:

$$\Delta\omega = \frac{-J_i^T w_i(\overline{\omega}_0) - J_r^T w_r(\overline{\omega}_0)}{J_i^T J_i + J_r^T J_r}, \quad (12)$$

where $J_i = [\partial w_i(\overline{\omega}_0)/\partial\overline{\omega}_0]$. $J_r = [\partial w_r(\overline{\omega}_0)/\partial\overline{\omega}_0]$. The several simulations show that the number of iterations I_t can be chosen to be 10. The local optimal solution $\overline{\omega}_{0,k}$ segmentation variable k can be obtained based on the range of $\overline{\omega}_0$. The restricted search criterion for choosing $\overline{\omega}_{0,k}$ is given as follows:

$$k_0 = \begin{cases} \min\limits_k J\left(A_{0c}, \overline{\omega}_{0,k}\right), \\ sinc\left(\dfrac{\overline{\omega}_{0,k} NT_s}{2}\right) > 0.1, \\ A_{0c}|_{\overline{\omega}_{0,k}} > 0, \end{cases} \quad (13)$$

where $\overline{\omega}_{0,k_0}$ is the estimated frequency parameter in the 2nd step. Above all, MF can be obtained from the fine MF estimation of the 2nd step.

3.3. Two-Step Frequency Estimation Method. The two-step frequency parameters estimation method is shown in Figure 1. The method can be depicted in more detail as follows:

(a) Calculating the search step of the initial frequency and chirping rate based on (5).

(b) In coarse search, the estimated value $(\widetilde{\alpha}_0, \widetilde{f}_0)$ can be obtained based on the threshold γ.

(c) In fine search, an iterative approach based on ML is adopted:

With frequency error $\Delta\overline{\omega}_0$ initialized, the amplitude can be obtained after calculating the amplitude

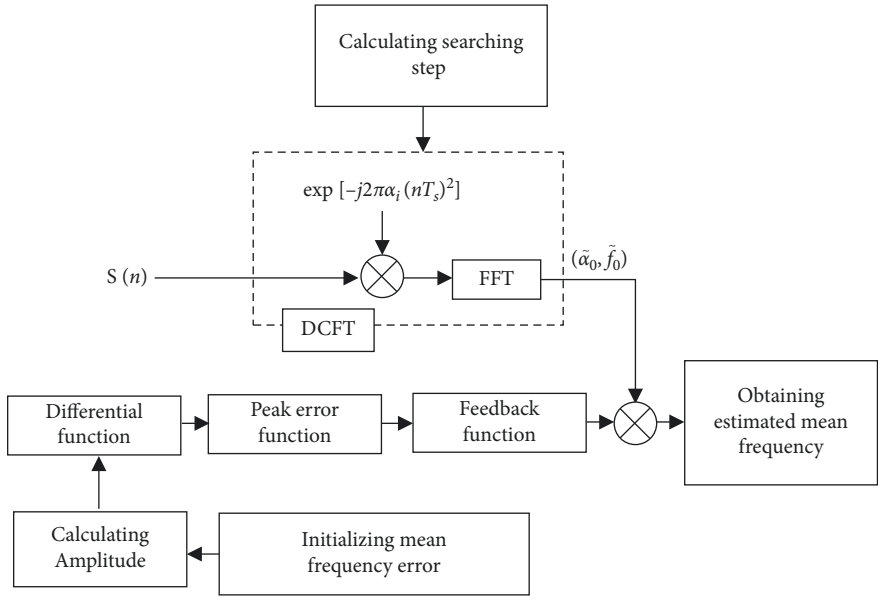

Figure 1: The two-step method's flow diagram combining DCFT for coarse frequency estimation and MLEP for fine frequency estimation.

function (9). Moreover, based on (Δ_T, δ_T), the range of $\overline{\omega}_0$ can be obtained.

Based on the amplitude and mean frequency error, the value of the differential functions J_i and J_r can be obtained as follows:

$$\begin{aligned} J_i &= \frac{\left(T_s * \left(TT1 * \mathrm{Im}\left(S_d\right) * T_c + TT1 * \mathrm{Re}\left(S_d\right) * T_s\right)\right)}{T_{2c}} - \frac{\left(TT1 * T_c * \left(\mathrm{Re}\left(S_d\right) * T_c - \mathrm{Im}\left(S_d\right) * T_s\right)\right)}{T_{2c}} \\ &\quad - \frac{\left(2 * TT1 * T_s * T_{2s} * \left(\mathrm{Re}\left(S_d\right) * T_c - \mathrm{Im}\left(S_d\right) * T_s\right)\right),}{T_{2c}^2} \\ J_r &= \frac{\left(T_c * \left(TT1 * \mathrm{Im}\left(S_d\right) * T_c + TT1 * \mathrm{Re}\left(S_d\right) * T_s\right)\right)}{T_{2c}} + \frac{\left(TT1 * T_s * \left(\mathrm{Re}\left(S_d\right) * T_c - \mathrm{Im}\left(S_d\right) * T_s\right)\right)}{T_{2c}} \\ &\quad - \frac{\left(2 * TT1 * T_c * T_{2s} * \left(\mathrm{Re}\left(S_d\right) * T_c - \mathrm{Im}\left(S_d\right) * T_s\right)\right)}{T_{2c}^2}, \end{aligned} \tag{14}$$

where $\mathrm{T}_c = \cos(TT1)$, $\mathrm{T}_s = \sin(TT1)$, $\mathrm{T}_{2c} = \cos(2TT1)$, $\mathrm{T}_{2s} = \sin(2TT1)$, and $TT1 = N - 1/2T_s\overline{\omega}_0$. The peak error functions $w_i(\overline{\omega}_0)$ and $w_r(\overline{\omega}_0)$ can be written as follows:

$$\begin{cases} w_i\left(\overline{\omega}_0\right) = \mathrm{Im}\left(S_d\left(k_0, \alpha_0\right)\right) - \dfrac{\mathrm{Re}\left(S_d\right)\cos\left(\overline{\omega}_0 N - 1/2T_s\right) - \mathrm{Im}\left(S_d\right)\sin\left(\overline{\omega}_0 N - 1/2T_s\right)}{\cos\left(\overline{\omega}_0 (N-1) T_s\right)} \sin\left(\overline{\omega}_0 \dfrac{N-1}{2} T_s\right), \\ w_r\left(\overline{\omega}_0\right) = \mathrm{Re}\left(S_d\left(k_0, \alpha_0\right)\right) - \dfrac{\mathrm{Re}\left(S_d\right)\cos\left(\overline{\omega}_0 N - 1/2T_s\right) - \mathrm{Im}\left(S_d\right)\sin\left(\overline{\omega}_0 N - 1/2T_s\right)}{\cos\left(\overline{\omega}_0 (N-1) T_s\right)} \cos\left(\overline{\omega}_0 \dfrac{N-1}{2} T_s\right), \end{cases} \tag{15}$$

where the unit (k_0, α_0) is corresponding to $(\tilde{\alpha}_0, \tilde{f}_0)$. Based on differential functions, peak error function and (11), feedback error $\Delta\omega$ can be obtained. The feedback function in Figure 1 can be written as follows:

$$\overline{\omega}_0 = \overline{\omega}_0 - \Delta\omega. \tag{16}$$

(d) Based on step (c), $\overline{\omega}_{0,k}$ can be obtained after 10 iterations. Then, based on (13), the final MF can be estimated. Above all, the frequency accuracy can be improved.

4. Algorithm Performance

In this section, Cramér–Rao bound of the estimated MF of the proposed method is derived. Then, computational burdens and detection probability of the proposed method are analyzed for performance evaluation.

4.1. Cramér–Rao Bound (CRB) of the Proposed Method. Based on the theory [17], the CRB of $\overline{\omega}_0$ can be written as follows:

$$CR_{\overline{\omega}_0} = \frac{1}{E\left(\partial^2\left((w_i)^2 + (w_r)^2/2\sigma_w^2\right)/\partial^2\overline{\omega}_0\right)} = \frac{2\sigma_w^2}{E}\left[\frac{\partial^2\left((w_i)^2 + (w_r)^2\right)}{\partial^2\overline{\omega}_0}\right], \tag{17}$$

where $w_i = \mathrm{Im}(S_d) - A_0\mathrm{sinc}(\overline{\omega}_0 NT_s/2)\sin(\overline{\omega}_0 N - 1/2T_s)$, and $w_r = \mathrm{Re}(S_d) - A_0\mathrm{sinc}(\overline{\omega}_0 NT_s/2)\cos(\overline{\omega}_0 N - 1/2T_s)$. When $\mathrm{sinc}(\overline{\omega}_0 NT_s/2) \approx 1$,

$$CR_{\overline{\omega}_0} \approx \frac{2\sigma_w^2}{\left[(N-1)^2 T_s^2 A_0^2\right]}, \tag{18}$$

where we can obtain the final CRB of $\overline{\omega}_0$. When $A_0 \approx N$, $\frac{s}{T} = 0.001\ s$, $N = 200$ ms, 400 ms and 600 ms, the CRB of MF is shown in Figure 2.

In Figure 2, CRB curves are shown with the integration time being 100, 200, and 300 ms, respectively. Under the same SNR, the longer the integration time is, the higher the frequency estimation accuracy is. This is because based on (19) the integration time is long, and the integration peak value is large.

4.2. Computations Analysis. Based on (2) and (10), the computations of the proposed method can be obtained. Here, the BASIC [11] is chosen as the benchmark for the coarse MF estimation. The method estimates the frequency parameters based on the differential signal as follows:

$$\begin{aligned} S_d(n) &= S^*(n)S(n + M_0) \\ &= A^2 b(n)b(n + M_0)\exp \\ &\quad \cdot \left[j2\pi\left(2n\mu M_0 T_s^2 + f_0 M_0 T_s + \mu M_0^2 T_s^2\right)\right] \\ &= A^2 b(n)b(n + M_0)\exp\left[j2\pi\left(2n\mu M_0 T_s^2 + \theta_0\right)\right], \end{aligned} \tag{19}$$

where $\theta_0 = f_0 M_0 T_s + \mu M_0^2 T_s^2$. Based on the Fourier transform, the frequency parameters can be estimated.

In Table 1, methods are chosen for coarse or fine MF estimation. T_α represents the number of chirping rate search bins and T_f represents the number of initial frequency search. $C_{P,M}$ and $C_{P,A}$ can be calculated as follows.

Firstly, A is calculated from (9). Calculating (9) involves 12 multiplications and 1 addition. Moreover, the value of cos () or sin () function can be realized by a look-up table, and their computations can be ignored. Then, calculating differential function costs $18 * 2$ multiplications and $2 * 2$ additions. Calculating the peak error function costs $5 * 2$ multiplications and $1 * 2$ additions. Hereafter, (12) costs 5 multiplications and 2 additions. Calculating the feedback function costs 1 addition. In addition, calculating (13) costs 19 multiplications and 3 additions.

Above all, one complex multiplication equals two multiplications [4]. So, $C_{P,M} = L_k(51I_i + 19)/2$ and $C_{P,A} = L_k(9I_i + 3)/2$, where I_t represents the number of iterations and L_k represents the number of segmentations. Besides, Table 1 shows that the frequency accuracy of the Schmidt method is also dependent on the number of vectors.

Since the computations simulation needs to set lots of simulation parameters, the simulation will be conducted in Section 5.

4.3. Detection Performance. Since the signal is detected in the first step of the proposed method, the section is to discuss the detection probability of the first step in the proposed method. The theoretical simulation will be conducted in Section 5.1.

The detection variable $|S_d(k_0, \alpha_0)|^2$ obeys the chi-square distribution. When the signal is absent or a wrong frequency bin is searched, $J_d = |S_d(k_0, \alpha_0)|^2$ obeys the central chi-square distribution with the variance σ_w^2, and the probability density function can be written as follows:

$$p_0(J_d) = \frac{1}{2\sigma_w^2}\exp\left(-\frac{J_d}{2\sigma_w^2}\right), \tag{20}$$

where p_0 represents probability density function when a wrong bin is searched. When the right frequency unit is detected, $J_d = |S_d(k_0, \alpha_0)|^2$ obeys the noncentral chi-square distribution with the variance σ_w^2, and the probability density function can be written as follows:

$$p_1(J_d) = \frac{1}{2\sigma_w^2}\exp\left(-\frac{J_d + {}^2_a}{2\sigma_w^2}\right) I_0\left(\sqrt{\frac{{}^2_a J_d}{\sigma_w^4}}\right), \tag{21}$$

where p_1 represents the probability density function when the right frequency bin is detected. Under an incorrect frequency hypothesis H_0, the false alarm probability P_{fa} can be written as:

$$\begin{aligned} P_{fa} &= P\{y \geq \gamma_D | H_0\} = 1 - \left(\int_0^{\gamma_D} p_0(y)\mathrm{d}y\right)^{T_f T_\alpha - 1} \\ &\approx 1 - \left(1 - \exp\left(-\frac{\gamma_D}{2\sigma_w^2}\right)\right)^{T_f T_\alpha - 1}, \end{aligned} \tag{22}$$

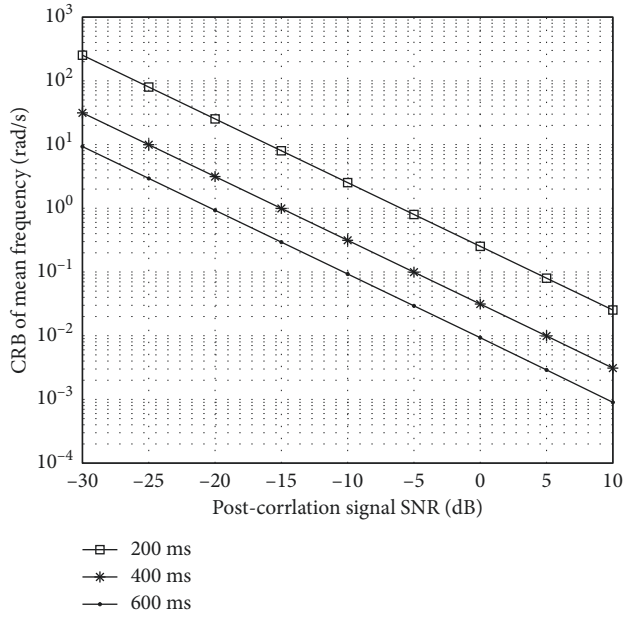

Figure 2: CRB of $\overline{\omega}_0$ under different integration times.

Table 1: Computational burdens comparison.

Coarse MF estimation	Complex multiplications	Complex additions
BASIC	$(T_\alpha) + (T_\alpha)/2\log_2(T_\alpha)$ $+(T_f) + T_f/2\log_2(T_f)$	$(T_\alpha)\log_2(T_\alpha)$ $+(T_f)\log_2(T_f)$
Proposed method (1st step)	$T_\alpha T_f/2\log_2(T_f)$	$T_\alpha T_f \log_2(T_f)$
Fine MF estimation	Complex multiplications	Complex additions
Proposed method(2nd step)	$N + C_{P,M}$	$C_{P,A}$
Schmidt method (appendix table 2) [5]	$\left(\begin{array}{c}(2N+1)(M+1)+\\ 1+2(M!)+\\ (M-1)!+\\ (N+1)\sum_{m=1}^{M} m!\end{array}\right)/2$	$0.5\left(\begin{array}{c}(N-1)(M+2)+\\ M(N+1)+(M-1)!+\\ (M-2)!+N\sum_{m=1}^{M} m!\end{array}\right)$

Table 2: computational burdens for the Schmidt method algorithm [5].

	Multiplications	Additions
$R(1,1) = P_1^2$	N	$N-1$
$R(k,1) = \overline{P_k P_1}$ $k = 1,...,M$	$1 + MN$	$M(N-1)$
$C(1) = \overline{yP_1}$	$N+1$	$N-1$
for$k = 1,\ldots,M$ for$i = 1,\ldots,k$ $k > iR(k,i) = \overline{P_k P_i} - \sum_{j=1}^{i-1}\alpha_{ji}R(k.j)$ $k = iR(k,k) = \overline{P_k P_k} - \sum_{j=1}^{k-1}\alpha_{jk}^2 R(j.j)$	$\sum_{m=1}^{M} m!(N+1)$	$\sum_{m=1}^{M} m!N$
for$k = 1,\ldots,M$ $C(k) = \overline{yP_k} - \sum_{j=1}^{k-1}\alpha_{jk}C(j)$	$MN + (M-1)!$	$MN + (M-2)!$
$g_k = C(k)/R(k,k)$	M	0
$\theta_i = g_i - \sum_{k=i+1}^{m} R(k,i)/R(i,i)\theta_k$ $i = 1,\ldots,M$	$2(M!)$	$(M-1)! + M$

M represents the number of vectors, and N represents the length of the vector. g_k represents coefficients of Schmidt orthogonalization.

where γ_D represents the detection threshold. Under the correct frequency hypothesis H_1, the detection probability P_D can be written as follows:

$$P_D = P\{x \geq \gamma_D | H_1\} = \int_{\gamma_D}^{+\infty} p_1(x)\left(\int_0^x p_0(y)\mathrm{d}y\right)^{T_f T_\alpha - 1}\mathrm{dx}, \tag{23}$$

where T_f represents the number of initial frequency search bins in the first step of the proposed method and T_a represents the number of chirping rate search bins. When the configured P_{fa} is small, $(\int_0^{J_d} p_0(J_d)dJ_d)^{T_f T_\alpha - 1} \approx 1$, and the detection probability P_D can be simplified into

$$P_D = P\{J_d \geq \gamma_D / H_1\} \approx Q\left(\frac{a}{\sigma_w}, \frac{\sqrt{\gamma_D}}{\sigma_w}\right), \tag{24}$$

where a equals to $|S_d(k_0, \alpha_0)|$ in the absence of noise. Based on the definition of miss detection probability [18], the miss probability of the proposed method can be written as:

$$P_M = \int_0^{\gamma_D} p_1(x)\left(\int_0^{\gamma_D} p_0(y)\mathrm{d}y\right)^{T_f T_\alpha - 1}\mathrm{dx}. \tag{25}$$

When the set P_{fa} is small, $(\int_0^{\gamma_D} p_0(J_d)dJ_d)^{T_f T_\alpha - 1} \approx 1$, $P_D + P_M = 1$. Above all, the detection probability of coarse MF estimation of the proposed method can be obtained. When the signal is detected, the second step of the proposed method for fine MF estimation can be performed.

5. Simulation Results

In this section, BASIC [11] and FRFT [13] are chosen as the benchmark for the 1st step of the proposed method, and Schmidt [5] is chosen as the benchmark for the 2nd step. The simulation parameters are listed in Table 3 where $\lceil \eta \rceil$ represents the smallest integer that is larger than η.

5.1. Coarse Frequency Detection Performance Comparison. Although complex multiplications of the proposed method for coarse MF estimation are larger than that of BASIC in Figure 3, when the SNR of the postcorrelation signal is larger than −10 dB, the detection probability of the proposed method is almost 100%, which is larger than other FRFT and BAISIC in Figure 4. This is because FRFT has a search bin α and BAISIC adopts a differential process, which may degrade the correlation peak and lead to lower detection probability.

5.2. Fine MF Accuracy and Complexity Comparison. Based on the simulation above, the DCFT method, two-step method, and Schmidt method are adopted for the fine MF search. In Figure 5, the complex multiplications of Schmidt vary greatly with the change of MF search step and postcorrelation signal length.

In Figure 6, even though 1 rad/s of MF search step is adopted for MF estimation, the two-step method based on

Table 3: simulation parameters.

Parameters	Value
Initial frequency range	(−250, 250) Hz
Chirping rate range	(−500, 500) Hz/s
Initial frequency search step (Δ_d)	$1/(2T_0) = 1/(2NT_s)$
Sampling time (T_s)	0.001 s
Factor (γ)	0.5
Number of iterations (I_t)	10
Number of segmentation (L_k)	$\lceil (4(N-1)T_s\overline{\omega}_{\max})/\pi \rceil$
Monte Carlo simulation	5000
Max mean frequency ($\overline{\omega}_{\max}$)	$2\pi\Delta_d + 2\pi\delta_d(N-1)/2T_s$
False alarm probability (P_{fa})	2×10^{-10}

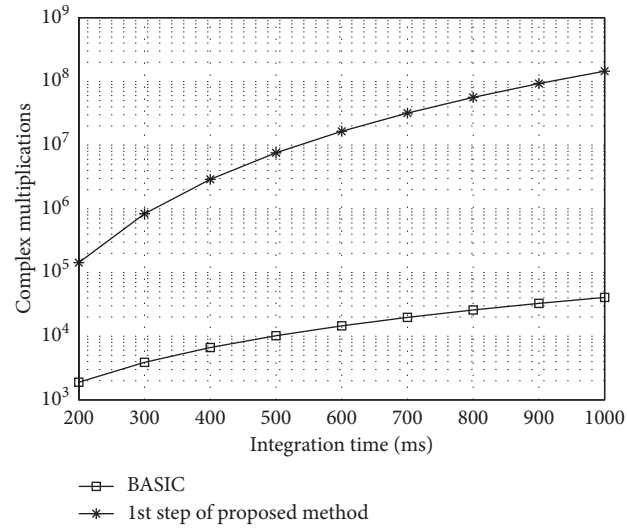

Figure 3: Complex multiplications comparison for coarse MF estimation methods.

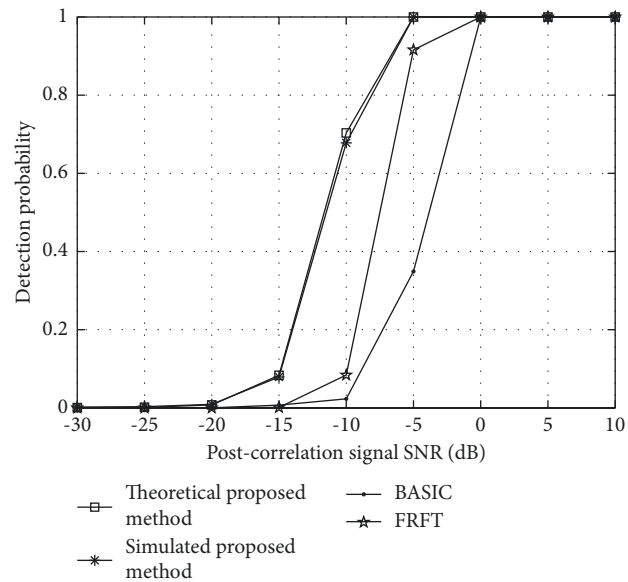

Figure 4: Detection probabilities comparison when is 200 ms, chirping rate is 200 Hz/s, and initial frequency is 100 Hz.

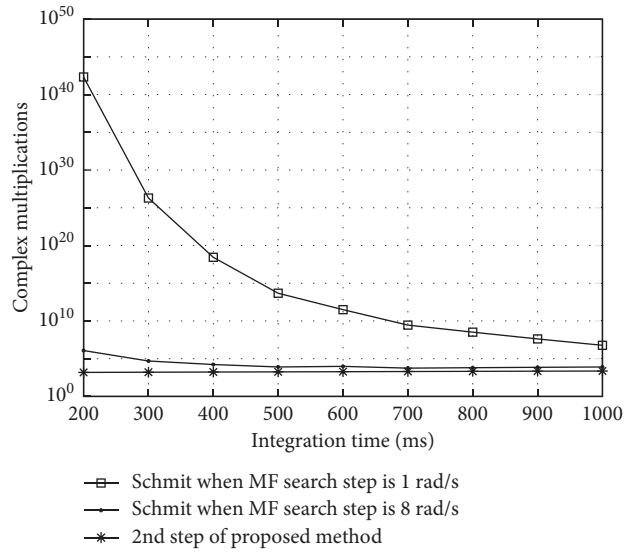

Figure 5: Complex multiplications comparison for fine MF estimation methods.

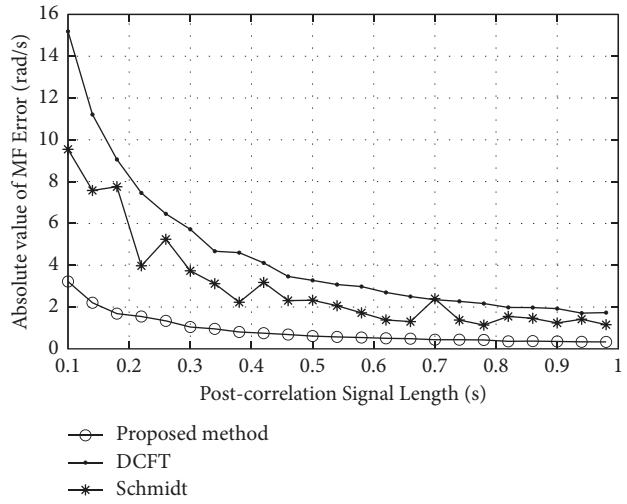

Figure 6: MF square error comparison. The SNR of the post-correlation signal is 5 dB. The MF search step is 1 rad/s. The integration time is 200 ms in coarse MF estimation.

MLEP gains higher precision than MF search based on Schmidt.

6. Conclusion

To improve frequency accuracy in high-dynamic acquisition, we propose a two-step frequency estimation method. The proposed method combines a coarse frequency estimation method based on DCFT and MLEP for fine frequency estimation. In the 1st step, the search step of initial frequency and chirping rate is configured based on Taylor expansion, and coarse MF is obtained. In the 2nd step, due to low-frequency error, fine MF is estimated by MLEP. Although DCFT costs much more computation in Figure 3 compared with BASIC, it improves the detection probability in Figure 4. Moreover, the proposed MLEP obtains higher mean frequency accuracy and lower complex multiplications compared with the conventional method Schmidt. Furthermore, in practice, the proposed two-step method can provide a theoretical basis for open-loop frequency tracking.

Data Availability

Due to laboratory requirements, the data cannot be made public.

Conflicts of Interest

The authors declare that they have no conflicts of interest.

Acknowledgments

Part of this work was supported by the National Natural Science Foundation of China under Grants 61901154 and 61971355; the Project of Guangxi Technology Base and Talent Special Project (No.GuiKe AD20159018), the Project of Guangxi Natural Science Foundation (No.2020GXNSFAA159004), Zhejiang Province Science Foundation for Youths under Grant LQ19F010006, and Beijing Natural Science Foundation under Grant no. 4214072.

References

[1] B. Parkinson, J. Spilker, and P. Axelrad, *Global Positioning System: Theory and Applications*, Amer. Inst. Aeronatics Astro, Washington, DC, 1996.

[2] C. Wu and Y. Gao, "Low-computation GNSS signal acquisition method based on a complex signal phase in the presence of sign transitions," *IEEE Transactions on Aerospace and Electronic Systems*, vol. 56, no. 6, pp. 4177–4191, 2020.

[3] S. Liu, T. Shan, R. Tao et al., "Sparse Discrete fractional fourier transform and its applications," *IEEE Transactions on Signal Processing*, vol. 62, no. 24, pp. 6582–6595, 2014.

[4] S. H. Kong, "SDHT for fast detection of weak GNSS signals," *IEEE Journal on Selected Areas in Communications*, vol. 33, no. 11, pp. 2366–2378, 2015.

[5] T. Mohamed and N. Aboelmagd, "Robust fine acquisition algorithm for GPS receiver with limited resources," *GPS Solutions*, vol. 20, no. 1, pp. 77–88, 2016.

[6] S. Liu, H. Zhang, T. Shan, and Y. Huang, "Efficient radar detection of weak manoeuvring targets using a coarse-to-fine strategy," *IET Radar, Sonar & Navigation*, vol. 15, no. 2, pp. 181–193, 2021.

[7] X. Tang, E. Falletti, and L. Lo Presti, "Fast nearly ML estimation of Doppler frequency in GNSS signal acquisition process," *Sensors*, vol. 13, no. 5, pp. 5649–5670, 2013.

[8] W. Kedong, "A new algorithm for fine acquisition of GPS carrier frequency," *GPS Solutions*, vol. 18, no. 4, pp. 581–592, 2014.

[9] N. Linty and L. Lo Presti, "Doppler frequency estimation in GNSS receivers based on double FFT," *IEEE Transactions on Vehicular Technology*, vol. 65, no. 2, pp. 509–524, 2016.

[10] T. T. Nguyen, V. T. La, and T. H. Ta, "A novel residual frequency estimation method for GNSS receivers," *Sensors*, vol. 18, no. 1, p. 119, 2018.

[11] C. Yang, T. Nguyen, and E. Blasch, "Post-correlation semi-coherent integration for high-dynamic and weak GPS signal acquisition (preprint)," in *Proceedings of the position, location*

and navigation symposium 2008 IEEE/ION, Monterey, CA, USA, May2008.

[12] Y. R. Luo, L. Zhang, and H. Ruan, "An acquisition algorithm based on FRFT for weak GNSS signals in A dynamic environment," *IEEE Communications Letters*, vol. 22, no. 6, pp. 1212–1215, 2018.

[13] Y. R. Luo, C. Y. Yu, S. H. Chen, J. Li, H. Ruan, and N. El-Sheimy, "A novel Doppler rate estimator based on fractional fourier transform for high-dynamic GNSS signal," *IEEE Access*, vol. 7, no. 1, pp. 29575–29596, 2019.

[14] C. Wu, L. P. Xu, H. Zhang, and W. Zhao, "A block zero-padding method based on DCFT for L1 parameter estimations in weak signal and high dynamic environments," *Frontiers of Information Technology & Electronic Engineering*, vol. 16, no. 9, pp. 796–804, 2015.

[15] T. Erseghe, P. Kraniauskas, and G. Carioraro, "Unified fractional Fourier transform and sampling theorem," *IEEE Transactions on Signal Processing*, vol. 47, no. 12, pp. 3419–3423, 1999.

[16] B. C. Geiger and C. Vogel, "Influence of Doppler bin width on GPS acquisition probabilities," *IEEE Transactions on Aerospace and Electronic Systems*, vol. 49, no. 4, pp. 2570–2584, 2013.

[17] H. Y. Zhang, L. P. Xu, B. Yan, H. Zhang, and L. Luo, "A carrier estimation method based on MLE and KF for weak GNSS signals," *Sensors*, vol. 17, no. 7, p. 1468, 2017.

[18] S. H. Kong, "A deterministic compressed GNSS acquisition technique," *IEEE Transactions on Vehicular Technology*, vol. 62, no. 2, pp. 511–521, 2013.